Available online at www.sciencedirect.com
SCIENCE DIRECT®
ELSEVIER
Ultramicroscopy 99 (2004) 87–94
ultramicroscopy
www.elsevier.com/locate/ultramic

Spectromicroscope for the PHotoelectron Imaging of Nanostructures with X-rays (SPHINX): performance in biology, medicine and geology

Bradley H. Frazer[a,b,*], Marco Girasole[c], Lisa M. Wiese[d], Torsten Franz[e], Gelsomina De Stasio[a,d]

[a] *Department of Physics, University of Wisconsin at Madison, Madison, WI 53706, USA*
[b] *Institute de Physique Appliquée Ecole Polytechnique Fédérale de Lausanne, CH-1015 Lausanne, Switzerland*
[c] *Instituto di Struttura della Materia del CNR, Via Fosso del Cavaliere, 1-00133 Roma, Italy*
[d] *University of Wisconsin Synchrotron Radiation Center, Stoughton, WI 53589, USA*
[e] *ELMITEC GmbH, Albrecht-von-Groddeck-Straße 3, D-38678 Clausthal-Zellerfeld, Germany*

Received 19 May 2003; received in revised form 15 September 2003; accepted 17 October 2003

Abstract

Several X-ray PhotoElectron Emission spectroMicroscopes (X-PEEMs) exist around the world at this time. We present recent performance and resolution tests of one of them, the Spectromicroscope for PHotoelectron Imaging of Nanostructures with X-rays (SPHINX) X-PEEM, installed at the University of Wisconsin Synchrotron Radiation Center. With this state-of-the-art instrument we demonstrate chemical analysis capabilities on conducting and insulating specimens of diverse interests, and an unprecedented lateral resolution of 10 nm with monochromatic X-rays and 7.2 nm with ultraviolet illumination.

Keywords: PEEM; X-PEEM

1. Introduction

PhotoElectron Emission spectroMicroscopy (PEEM) is a full field imaging technique that, when combined with the tunable X-ray radiation from synchrotron sources (X-PEEM), provides a surface sensitive spectroscopy on the micro- and nano-scopic level, also known as spectromicroscopy. Starting with the pioneering work of Tonner and Harp [1], instrumental development has been rapid and the number of applications of X-PEEM have increased dramatically. X-PEEM now makes significant contributions to the fields of thin film magnetism, semiconductor technology, polymer science, geology, microbiology, and medicine [2–15]. Instrumental development has been strongly motivated by the ever increasing demand for high spatial resolution and sensitivity.

Typically, an X-PEEM consists of a sample held at high voltage followed by a series of electron

*Corresponding author. Department of Physics, Synchrotron Radiation Center, University of Wisconsin at Madison, 3731 Schneider Dr., Stoughton, WI 53589, USA. Tel.: 6088772366; fax: 6088772001.
E-mail address: bhfrazer@wisc.edu (B.H. Frazer).

0304-3991/$ - see front matter © 2003 Elsevier B.V. All rights reserved.
doi:10.1016/j.ultramic.2003.10.001

optics, a microchannel plate and a phosphor screen. The electron optics can be either electrostatic or magnetic and often include a series of deflectors and stigmators. In most cases the electron optics are optimized for low energy secondary electrons but several modern X-PEEMs now incorporate energy filtering capability to select primary photoelectrons or Auger electrons for imaging [16,17].

The SPHINX (Spectromicroscope for PHotoelectron Imaging of Nanostructures with X-rays) X-PEEM is manufactured by ELMITEC GmbH (Clausthal, Germany, www.elmitec-gmbh.com, model PEEM III) and consists of six magnetic lenses: an objective, a transfer, a field, an intermediate and two projective lenses.

Additionally, two stigmators and five deflectors are placed at appropriate locations (see Fig. 1)

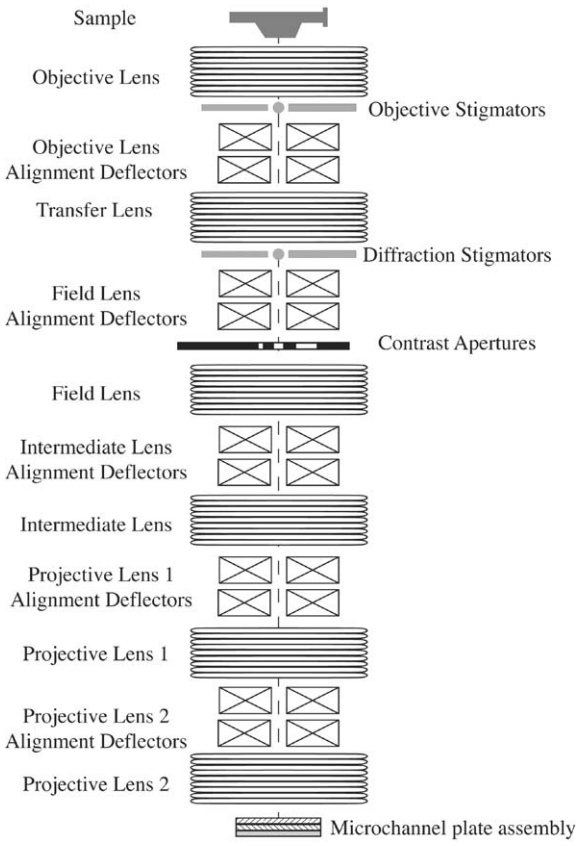

Fig. 1. Schematic view of the SPHINX electron optics configuration.

along the electron optical path, to correct for misalignment of the magnetic lenses and provide precise focusing. Three apertures with diameters 100, 50, and 30 μm can be inserted in the optics column in a conjugated plane to the back focal plane of the objective lens. At this location the focal plane is demagnified by a factor of two with respect to the back focal plane of the objective lens and the aperture reduces the contribution of off-axis electrons. The magnified photoelectron image is focused onto two microchannel plates and converted into a visible image by a phosphor screen. The image is then collected by a slow scan 12 bit digital camera and transferred to a computer using custom acquisition software. The optics column is capable of a maximum magnification of approximately 24,000×, with a field of view variable between 200 μm and 1.7 μm. These fields of view are accurately calibrated measuring an SEM reference sample with feature sizes ranging between 30 μm and 500 nm. The sample is held at −20.0 kV and illuminated at grazing incidence (16°) by X-rays from a synchrotron beamline, or by a near ultraviolet (UV) source (ORIEL model 6000, 100 W Hg arc lamp), mounted in a symmetric position with respect to the sample normal. The optics column is perpendicular to the sample surface. The sample manipulator, adjustable for x, y, z and tilt, enables sample heating to 1200°C as well as cooling to approximately 120 K. The microscope chamber is held at a base pressure of 10^{-10} Torr, while transfer of a sample from atmospheric pressure to the microscope chamber takes less than 1 h.

The SPHINX microscope is moved from one beamline to another on a 3-week basis, to accommodate different experiments requiring access to different energy ranges, energy resolutions and flux densities.

The ultimate spatial resolution of any PEEM is determined by spherical and chromatic aberrations of the objective lens [18]. The kinetic energy distribution of the secondary electrons produced by X-ray illumination may be several eV wide. A near ultraviolet (UV) source will result in low energy (<1 eV) and thus nearly monochromatic electrons. Spatial resolution is dominated by chromatic aberration and is therefore lower when

using an X-ray source. Chromatic aberration can be minimized by placing the microscopic aperture at a crossover point in the back focal plane of the objective lens. This reduces the contribution of faster electrons but is accompanied by a corresponding reduction in flux. Several X-PEEM groups have designed aberration correction electron optics [19–23] which will improve both transmission and resolution but at the time of writing, such optics have yet to be successfully implemented.

2. Results and discussion

Figs. 2–4 show SPHINX data that demonstrate the performance of the instrument in diverse fields of research. These data demonstrate the breadth and flexibility of X-PEEM when used over a broad energy range. In each case the optimized sample preparation and the data processing strategy are described. Fig. 2a presents an image of cyanobacteria in a calothrix filament: the direct SPHINX image of cyanobacteria, taken at 135 eV photon energy on the 071 undulator plane grating monochromator (PGM) beamline at the University of Wisconsin, Synchroton Radiation Center (SRC). Fig. 2a is the average of 10 images, each acquired

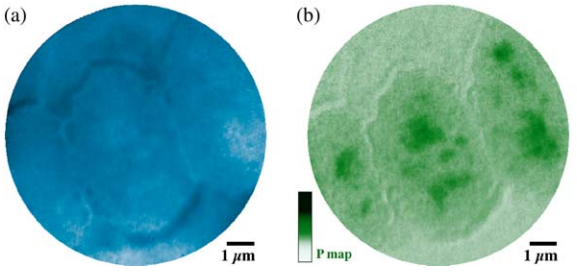

Fig. 2. (a) Direct SPHINX image of cyanobacteria in a calothrix filament (sample from Susanne Douglas of JPL, NASA), taken at 135 eV photon energy. The bacterium at the center of the image is adjacent to two other bacteria in the same filament, top-right and bottom-left, partly included in the image. The bacteria filaments were fixed, embedded in epoxy, ultramicrotomed to 60 nm sections, deposited on a silicon wafer and ashed for 42 h. (b) Phosphorus distribution map of the same bacteria in (a). The P map is obtained by digital ratio of an image at 139 eV to an image at 135 eV. SPHINX was installed on the PGM beamline at the SRC. The energy range of the PGM is 12–240 eV.

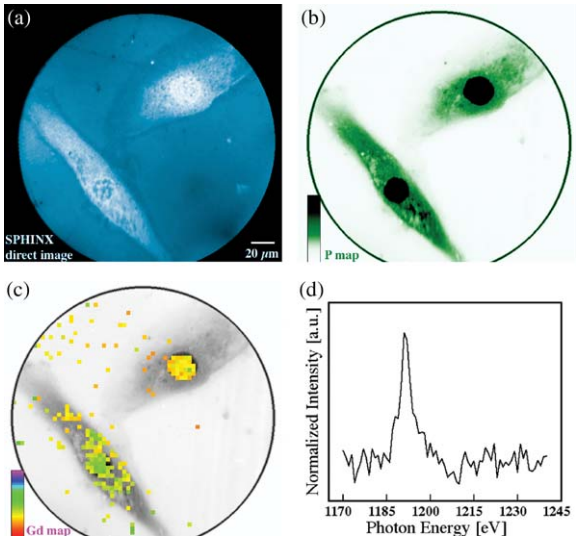

Fig. 3. Low-resolution high-sensitivity Gd mapping: (a) direct SPHINX image acquired at 1200 eV of human glioblastoma cells grown on a silicon wafer and exposed to a Gd compound (100 μM HM-Gd-DOTA) for 24 h, washed, fixed and ashed; (b) P distribution map obtained by ratio of images at 139 and 135 eV, highlighting in black the P-rich nuclei of the same two cells; (c) Gd location map (overlaid on a grayscale P map) extracted from a Gd movie as described in the text. To extract this map the movie was binned 8×8, therefore a single pixel is $8\,\mu m^2$; and (d) Gd M_5-edge spectrum extracted from a single pixel of the Gd movie. For these experiments SPHINX was installed on the 033 HERMON beamline at the SRC (energy range 62–1360 eV).

with a camera exposure time of 4 s. The 16 bit image contains 1280×1024 pixels, and was acquired with a sample voltage of -20 kV, a sample distance from the objective lens of 2 mm, an objective lens current of 1850 mA, a microchannel plate voltage of 1245 V, and a field of view of 10 μm. The contrast aperture used in this and all subsequent images was 30 μm.

Fig. 2b shows the phosphorus distribution map in the same area of Fig. 2a. The P map was obtained by digital ratio of images at 139 eV (P 2p on-peak) and 135 eV (off-peak).

The images in Fig. 2 were processed in NIH Image 1.62 [24], then converted to color with Adobe Photoshop 7. The P map of Fig. 2b shows a higher concentration of P in several areas within each bacterium. These areas correspond to high density of P-rich DNA. Most physiological ele-

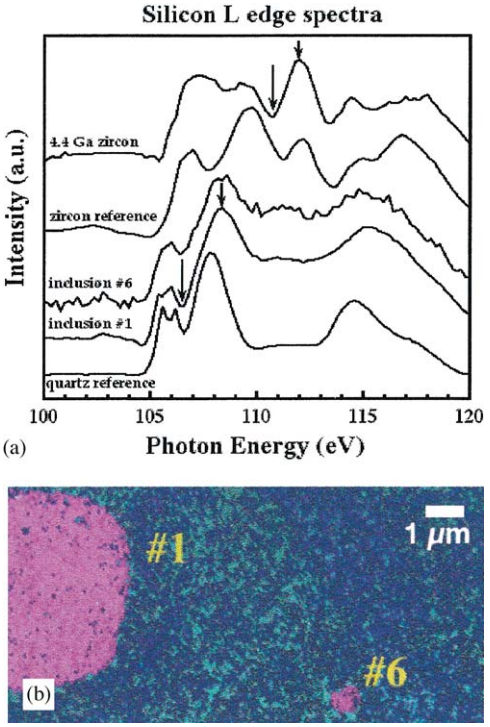

Fig. 4. Analysis of inclusions in a 4.4 billion-year-old zircon from Western Australia [11,29]. (a) Si L-edge spectra, from the top: SPHINX spectrum extracted from a $2 \times 2\,\mu m^2$ region of zircon; zircon reference spectrum [10]; SPHINX spectrum from inclusion #6 (circular region, 800 nm diameter); SPHINX spectrum from inclusion #1 ($2 \times 3\,\mu m^2$ rectangular region); reference quartz spectrum [10]. The arrows indicate the energies of the on-peak and off-peak images used to obtain the maps in b. (b) Distribution maps of quartz (magenta) and zircon (blue), extracted from SPHINX silicon movies, and superimposed on the direct image (cyan) [11].

ments in bacteria, as well as eukaryotic cells or tissue sections, are routinely mapped with SPHINX at high magnification, as in Fig. 2. These elements, and their corresponding edges are Na 2p at 33 eV, S 2p at 165 eV, Cl 2p at 202 eV, K 2p at 297 eV, Ca 2p at 350 eV, Fe 2p at 702 eV, Na 1s at 1070 eV.

Physiological elements and their localization at the subcellular level can be studied with SPHINX. If the elements listed above, and many others, are present in trace concentrations, the cells can be ashed in UV–ozone atmosphere as described in Refs. [25,26]. This is performed at room temperature and pressure, to remove carbon and therefore effectively enhance the concentration of other elements by a factor of 10, without displacing their microscopic localization. All the aforementioned elements can be easily mapped as in Fig. 2b after ashing.

Fig. 3 shows two human glioblastoma cells imaged with SPHINX, the P distribution map, a Gd location map and a single pixel Gd spectrum. In this case the goal of the experiment was to localize Gd in the cancer cell nuclei, to optimize Gd neutron capture therapy [27]. The cells were exposed to a Gd compound, and the bulk Gd concentration in these cells is on the order of 1–100 ppm. In this case we only use the lowest possible magnification, to maximize the Gd signal per unit area. Furthermore, to localize Gd at the subcellular level, the digital ratio map discussed above cannot be used. The pixel noise is often on the same order of magnitude as the Gd peak intensity. In addition, the pixel noise is not constant across the image area. We therefore extract the chemical information with an alternative strategy, described at length in Ref. [28]. Briefly, we acquire a stack of images (71 images, between 1200 and 1130 eV, 1 eV step) for Gd 3d and mount these in a "movie" using NIH Image 1.62. We then bin the stack 8×8 pixels to further increase the signal to noise ratio and to minimize calculation time. We then extract a Gd 3d spectrum from each pixel, normalize it, measure the signal intensity (Gd $3d_{5/2}$ peak area) and the noise level (in a well defined pre-peak region) and calculate the signal to noise ratio (R). If this ratio exceeds a pre-determined value ($R>18$) we retain the pixel as Gd-containing, if $R<18$ we reject the pixel. For all the retained pixels we then display the signal intensity in spectrum colors. We repeat the operation on a second movie acquired on the same region, and finally retain only the Gd-pixels that were reproducible in both Gd-location maps. A typical result of this analysis is presented in Fig. 3c.

In Fig. 4 we present an example of SPHINX chemical mapping obtained on the oldest rock found on Earth, a 4.4 billion year old zircon discovered in the Jack Hills region of Western Australia [29]. The zircon crystal (insulator) is embedded in epoxy (also insulating) and requires

coating with 10 Å Pt/Pd to be analyzed with SPHINX, as described in Ref. [11]. Fig. 4 proves that the zircon contains quartz inclusions down to 800 nm in size. The distribution maps of Fig. 4b for zircon and quartz were obtained by digital ratio of two images, on-peak and off-peak, at photon energies chosen to highlight quartz or zircon at the Si 2p edge. The quartz map was obtained by digital ratio of two images acquired at 108.4 and 106.4 eV photon energy. The zircon map is the ratio of images at 112.0 and 110.4 eV. The results of the mapping are verified by ensuring that spectra extracted from highlighted areas are in agreement with reference spectra for quartz and zircon as shown in Fig. 4a [10].

Note that quartz and zircon are both silicates; i.e., Si is present in both minerals as SiO_2 tetrahedra, for which the oxidation state of Si and the coordination number do not vary. They can be distinguished because of their different XANES spectral lineshapes due to different crystal structure.

While silicate minerals provide an excellent demonstration of the success of this coating approach, the technique allows X-PEEM analysis of any kind of insulating surface. Sample flatness is a requirement, but we do not have accurate measurements of the degree of surface roughness that we can or cannot image with X-PEEM. However, we recently tested the sputter coating approach on 20 μm diameter cells with a relief at the edges and the center of the cells of approximately 200 nm and 2 μm from the underlying silicon wafer, respectively, without major image distortion. In the presence of sharp edges, however, the X-PEEM imaging capability rapidly degrades.

For the resolution tests of Fig. 5, SPHINX was installed on the PGM beamline at the SRC. The PGM is one of the highest photon flux beamlines at the SRC, and this enabled high magnification and high resolution testing. The flux density on the PGM beamline is 4.0×10^8 photons per second per μm^2 at 100 eV and ΔE=160 meV.

Fig. 5 shows a photoelectron micrograph of gadolinium gallium garnet particles mixed with indium powder and pressed to 3000 pounds per square inch on a polished stainless steel die. This sample was chosen for the high contrast between the garnet particles and the indium substrate. Many particles smaller than 50 nm in this sample were resolved. Additionally, surface topography in combination with the grazing incidence of the X-ray photons created shadowed regions in the photoelectron image. Fig. 6 shows a region of this sample where deformations in the indium have created shadowed valleys.

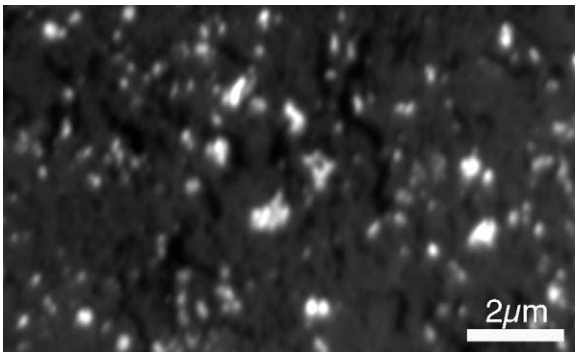

Fig. 5. Photoelectron micrograph of gadolinium gallium garnet ($Gd_3Ga_5O_{12}$) particles mixed with indium powder and pressed. Photon energy was 100 eV.

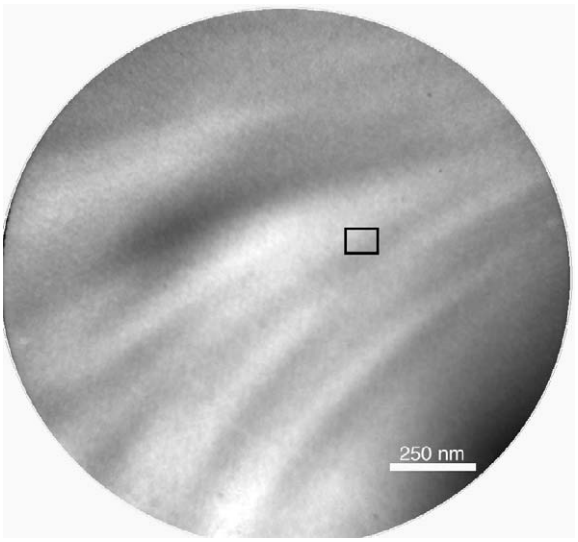

Fig. 6. Photoelectron micrograph of ridges produced by deformation of the indium surface, acquired at 100 eV photon energy. The black box highlights the region from which the line plots of Fig. 7 were extracted. Each pixel corresponds to 3.2 nm.

Multiple line plots across the diagonal of the highlighted region in Fig. 6 were performed and the resolution determined by using the Rayleigh criterion of the FWHM of the Gaussian fit derivative of a knife-edge. Rigorously, this corresponds to the distance between the 12% and 88% intensity points of the line plot acquired on a knife-edge feature. Fig. 7a shows six adjacent line plots all of which indicated less than 15 nm resolution. The highest resolution we obtained was 9.5 nm as illustrated in Fig. 7b. The resolutions measured on the adjacent line plots average to 11.7 nm. We conclude that with monochromatic X-rays the optimum resolution of the SPHINX X-PEEM is approximately 10 nm.

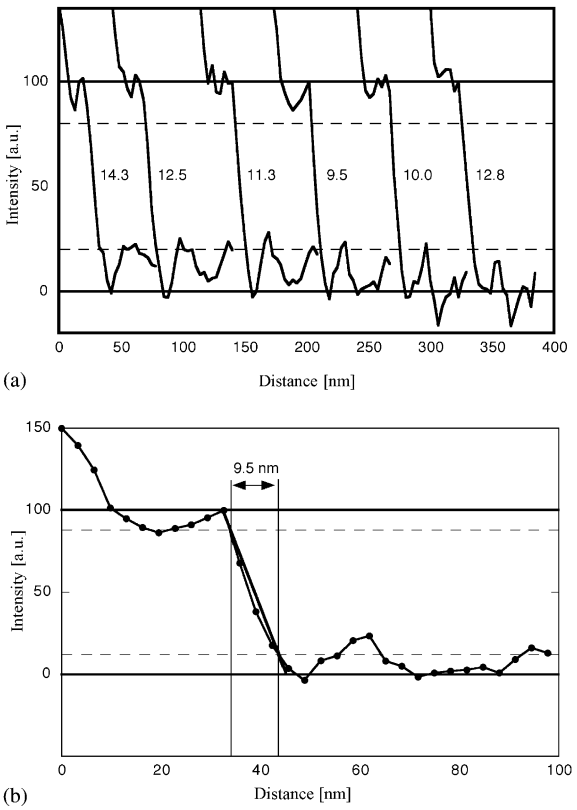

Fig. 7. (a) Six sequential line plots starting three pixels to the left and ending two pixels to the right of the diagonal of the box region of Fig. 6 (taken upper left to lower right). Numeric values indicate the distance between the 12% and 88% intensity points of each line plot. (b) Line plot of the knife-edge across the diagonal of the box region of Fig. 6.

To our knowledge this is the highest reported resolution for X-PEEM using monochromatic X-ray illumination.

The high-pressure mercury arc lamp provides UV light with a maximum photon energy of 4.96 eV. Since this is just above the work function of most materials, photoelectrons leave the sample with near-zero kinetic energy. This dramatically reduces the chromatic aberration of the objective lens and thereby improves the lateral resolution of the PEEM. Fig. 8 shows an image of lead islands on silicon acquired with the UV lamp. The Pb-islands sample was selected because of the high Pb–Si contrast in UV.

The line plot acquired along the black line in Fig. 9 is plotted in Fig. 10. The full-width at half-maximum of the lead island measures 7.2 nm. This is about 30% better than the result with X-ray illumination and illustrates the large effect of chromatic aberration in degrading lateral resolution. Several features are present in this line scan (and in adjacent line scans, not shown) that appear to be smaller than 7 nm. Since we are at the highest magnification of the microscope, the signal to noise ratio is poor, due to the limited photon flux

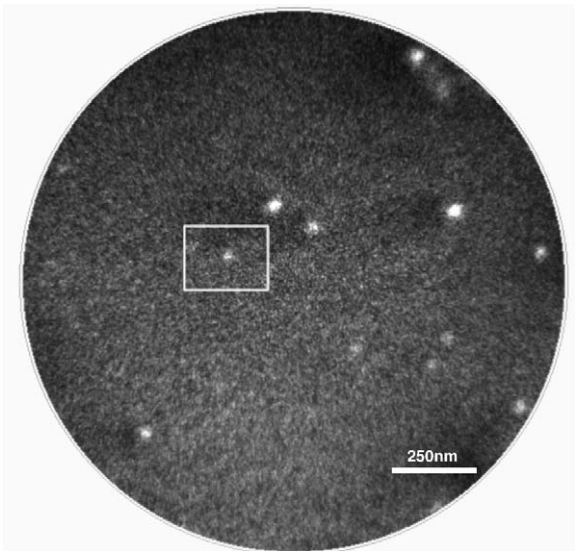

Fig. 8. SPHINX image of lead islands on a silicon wafer acquired under UV illumination. The box indicated the region of Fig. 9. Each pixel corresponds to 3.2 nm. The acquisition time was 1 s.

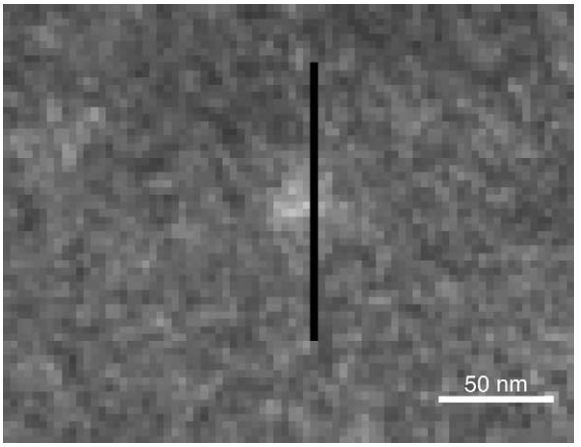

Fig. 9. Magnified view of the highlighted region of Fig. 8. The black line across the Pb island indicates where the line plot of Fig. 10 was acquired.

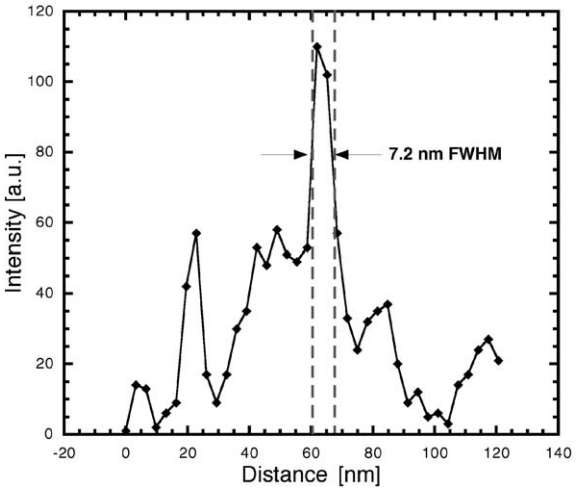

Fig. 10. Line plot acquired along the line in Fig. 9, showing a full-width at half-maximum of 7.2 nm.

of the UV lamp. Single pixel noise is therefore significant. While other line plots in this region showed smaller features, we chose this line plot as a resolution measurement because of its relatively low noise and more reliable lineshape. Note that it was not possible to obtain an image with UV illumination on the same sample and region of Fig. 6 because the signal and contrast were too low.

Manufacturing tolerances and magnetic inhomogeneities in the construction of an objective lens vary across instruments and result in different resolutions. These results are still inferior to the theoretical limits of approximately 5 nm for magnetic [30] and electrostatic [18] objective lenses, but illustrate the precision and high quality construction of this device.

3. Conclusions

We have presented data on very diverse samples including cyanobacteria, cancer cells, and silicates demonstrating the chemical analysis performances of the SPHINX spectromicroscope on conductors and insulators. We discussed resolution tests using X-rays and UV as illuminating sources. In conclusion, high resolutions in the 10 s of nanometer range can be achieved with this instrument on a variety of samples, provided the sample is flat. If the analyte concentration is very low, as in the case of Gd, the resolution must be traded for signal intensity, and only lower magnifications can be utilized. On very specific samples, with particularly high contrast, we obtained unprecedented spatial resolutions of 10 nm with X-rays and 7.2 nm with UV illumination.

Acknowledgements

We are indebted to Professor Ernst Bauer for his invaluable expertise and advice in the selection of the SPHINX microscope. We thank Czeslaw Koziol, Florian Schuetz and the staff at ELMITEC for their extraordinary technical support and for producing such a superb instrument. The experiments were performed at the Synchrotron Radiation Center, University of Wisconsin-Madison, which is supported by the NSF under Award No. DMR-0084402.

We acknowledge the financial support of the UW-Graduate School, UW-Physics Department, UW-Technology Innovation Fund-University Industry Relations, the UW-Comprehensive Cancer Center. One of us (M.G.) acknowledges the Italian CNR short-term mobility grant.

References

[1] G. Harp, B.P. Tonner, Rev. Sci. Instr. 59 (1988) 853.
[2] C. Schneider, G. Schönhense, Rep. Prog. Phys. 65 (2002) R1785.
[3] M.R. Freeman, B.C. Choi, Science 294 (2001) 1484.
[4] F. Nolting, A. Scholl, J. Stöhr, J.W. Seo, J. Fompeyrine, H. Siegwart, J.-P. Locquet, S. Anders, J. Lüning, E.E. Fullerton, M.F. Toney, M.R. Scheinfein, H.A. Padmore, Nature 405 (2000) 767.
[5] M. Kim, M. Bertram, M. Pollmann, A. von Oertzen, A.S. Mikhailov, H.H. Rotermund, G. Ertl, Science 292 (2001) 1357.
[6] F.J. Meyer zu Heringdorf, M.C. Reuter, R.M. Tromp, Nature 412 (2001) 517.
[7] S. Aggarwal, A.P. Monga, S.R. Perusse, R. Ramesh, V. Ballarotto, E.D. Williams, B.R. Chalamala, Y. Wei, R.H Reuss, Science 287 (2000) 2235.
[8] C. Morin, H. Ikeura-Sekiguchi, T. Tyliszczak, R. Cornelius, J.L. Brash, A.P. Hitchcock, A. Scholl, F. Nolting, G. Appel, D.A. Winesett, K. Kaznacheyev, H. Ade, J. Electron Spectrosc. Relat. Phenom. 121 (2001) 203.
[9] H. Ade, D.A. Winesett, A.P. Smith, S. Anders, T. Stammler, C. Heske, D. Slep, M.H. Rafailovich, J. Sokolov, J. Stöhr, Appl. Phys. Lett. 73 (1998) 3775.
[10] B. Gilbert, B.H. Frazer, F. Naab, J. Fournelle, J.W. Valley, G. De Stasio, Amer. Mineral. 88 (2003) 763.
[11] G. De Stasio, B.H. Frazer, B. Gilbert, K.L. Richter, J.W. Valley, Ultramicroscopy 198 (2003) 57.
[12] M. Labrenz, G.K. Druschel, T. Thomsen-Ebert, B. Gilbert, S.A. Welch, K.M. Kemner, G.A. Logan, R.E. Summons, G. De Stasio, P.L. Bond, B. Lai, S.D. Kelly, J.F. Banfield, Science 290 (2000) 1744.
[13] G. De Stasio, P. Casalbore, R. Pallini, B. Gilbert, F. Sanita', M.T. Ciotti, G. Rosi, A. Festinesi, L.M. Larocca, A. Rinelli, D. Perret, D.W. Mogk, P. Perfetti, M.P. Mehta, D. Mercanti, Cancer Res. 61 (2001) 4272.
[14] G. De Stasio, M. Capozi, G.F. Lorusso, P.A. Baudat, T.C. Droubay, P. Perfetti, G. Margaritondo, B.P. Tonner, Rev. Sci. Instr. 69 (1998) 2062.
[15] G. De Stasio, L. Perfetti, B. Gilbert, O. Fauchoux, M. Capozi, P. Perfetti, G. Margaritondo, B.P. Tonner, Rev. Sci. Instr. 70 (1999) 1740.
[16] A. Oelsner, O. Schmidt, M. Schicketanz, M. Klais, G. Schönhense, V. Mergel, O. Jagutzki, H. Schmidt-Böcking, Rev. Sci. Instr. 72 (2001) 3968.
[17] C. Quitman, U. Flechsig, L. Patthey, T. Schmidt, G. Ingold, M. Howells, M. Janousch, R. Abela, Surf. Sci. 480 (2001) 173.
[18] G.F. Rempfer, O.H. Griffith, Ultramicroscopy 27 (1989) 273.
[19] G.F. Rempfer, J. Appl. Phys. 67 (1990) 6027.
[20] W.P. Skoczylas, G.F. Rempfer, O.H. Griffith, Ultramicroscopy 36 (1991) 252.
[21] R. Fink, M.R. Weiss, E. Umbachl, D. Preikszas, H. Rose, R. Spehr, P. Hartel, W. Engel, R. Degenhardt, R. Wichtendahl, H. Kuhlenbeck, W. Erlebach, K. Ihmann, R. Schlögl, H.-J. Freund, A.M. Bradshaw, G. Lilienkamp, Th. Schmidt, E. Bauer, G. Benner, J. Electron Spectrosc. Relat. Phenom. 84 (1997) 231.
[22] G. Schönhense, H. Spiecker, J. Vac. Sci. Technol. B 20 (2002) 2526.
[23] J. Feng, H. Padmore, D.H. Wei, S. Anders, Y. Wu, A. Scholl, D. Robin, Rev. Sci. Instr. 73 (2002) 1514.
[24] Available online at http://rsb.info.nih.gov/nih-image/.
[25] G. De Stasio, B. Gilbert, L. Perfetti, R. Hansen, D. Mercanti, M.T. Ciotti, R. Andres, V.E. White, P. Perfetti, G. Margaritondo, Anal. Biochem. 266 (1999) 174.
[26] B. Gilbert, L. Perfetti, R. Hansen, D. Mercanti, M.T. Ciotti, P. Casalbore, R. Andres, P. Perfetti, G. Margaritondo, G. De Stasio, Front. Biosci. 5 (2000) 10.
[27] G. De Stasio, P. Casalbore, R. Pallini, B. Gilbert, F. Sanità, M.T. Ciotti, G. Rosi, A. Festinesi, L.M. Larocca, A. Rinelli, D. Perret, D.W. Mogk, P. Perfetti, M.P. Mehta, D. Mercanti, Cancer Res. 61 (2001) 4272.
[28] B.H. Frazer, B.R. Sonderegger, B. Gilbert, K.L. Richter, C. Salt, L. Wiese, D. Rajesh, S.P. Howard, J.F. Fowler, M.P. Mehta, G. De Stasio, Proceedings of the 2002 X-ray Microscopy Conference, J. Phys. IV 104 (2003) 349.
[29] S.A. Wilde, J.W. Valley, W.H. Peck, C.M. Graham, Nature 409 (2001) 175.
[30] J. Chmelik, L.H. Veneklasen, G. Marx, Optik 5 (1989) 155.